Experimental Investigation on the Facesheet Perforation Geometry on SDOF Acoustic Liner Impedance

Experimental Investigation on the Facesheet Perforation Geometry on SDOF Acoustic Liner Impedance

Felipe R. Rossi*, Lucas A. Bonomo† and Julio A. Cordioli‡
Federal University of Santa Catarina, Florianópolis - SC, 88040-900, Brazil

Francesco Avallone§
Politecnico di Torino, 10129, Torino, Italy

This work experimentally investigates the effects of facesheet perforation geometry on the acoustic impedance of Single-Degree-Of-Freedom (SDOF) liners. Four liner samples with the same nominal percentage of open area and cavity geometry were manufactured, differing only in the perforation shape: sharp-edged, outside chamfered, inside chamfered, and double chamfered, keeping the inner diameter constant. The actual perforation dimensions were assessed through optical characterization. The liner impedance was evaluated at the Liner Impedance Test Rig of the Federal University of Santa Catarina using two experimental approaches: inverse impedance eduction and the in-situ technique. Measurements were performed for centerline Mach numbers up to 0.50 and sound pressure levels of 130 and 145 dB over the frequency range from 500 to 3000 Hz. The results show that the liner reactance is only weakly affected by the perforation geometry for the conditions considered. In contrast, the resistance is sensitive to the perforation shape, specially under conditions in which nonlinear effects are relevant. In the absence of grazing flow, chamfered perforations mitigate the nonlinear resistance increase observed at high sound pressure levels. With grazing flow, the resistance becomes primarily dominated by flow-induced nonlinearities, and configurations with an outside chamfer tend to exhibit lower resistance than the sharp-edged configuration. Overall, the measurements indicate that perforation-edge geometry can affect the resistance of SDOF liners more significantly than the reactance within the range of conditions investigated.

I. Introduction

The treatment of the tonal component of fan noise in modern turbofan-powered aircraft remains a major aspect of the aircraft certification process. Since the early years of the turbofan era, acoustic liners installed in the nacelle have been the gold standard for tonal fan noise mitigation. The most typical acoustic liner design for turbofan applications, namely the Single-Degree-Of-Freedom (SDOF) liner, consists of a perforated facesheet backed by a honeycomb-like cavity structure, thus emulating an array of Helmholtz resonators. This configuration provides high attenuation over a narrow frequency band, which is usually tuned to match the fan Blade Passing Frequency (BPF) and its harmonics, corresponding to the dominant tonal-noise frequencies [1].

While the hole diameters in a liner perforated facesheet are on the order of millimeters, the nacelle dimensions (and the wavelengths of the dominant propagating modes) are on the order of meters. Therefore, it is still impractical to represent acoustic liners explicitly in acoustic numerical and/or analytical models [2]. The common approach is to represent the liner through its locally reactive, frequency-dependent complex acoustic impedance, $\tilde{Z}(\omega)$, which can then be used as a boundary condition in numerical and analytical models. The real component of the impedance is associated with dissipative mechanisms, which are usually related to the properties of the perforated facesheet. In contrast, the imaginary component, namely the reactance, is associated with inertial effects and is governed mainly by the cavity depth.

The impedance of acoustic liners is known to depend primarily on their geometry, but also on the operating conditions, namely the Sound Pressure Level (SPL), the grazing-flow velocity, and the boundary layer over the perforated facesheet [3, 4]. Given the complexity of this multiphysics problem, the determination of acoustic liner impedance is

*MSc Student, Department of Mechanical Engineering, felipe.rossi@lva.ufsc.br.
†Aeroacoustics Researcher Fellow, Department of Mechanical Engineering, lucas.bonomo@lva.ufsc.br, AIAA Member.
‡Associate Professor, Department of Mechanical Engineering, julio.cordioli@ufsc.br, AIAA Member.
§Full Professor, Departmento of Mechanical and Aerospace Engineering, francesco.avallone@polito.it, AIAA Member.

still primarily an experimental task, although high-fidelity numerical models are becoming a feasible alternative [2, 5]. Semi-empirical models have also been widely used to estimate the acoustic impedance, especially during the early stages of liner design [6]. A key aspect of these models is the assumption of sharp-edged holes in the perforated facesheet, i.e., perfectly cylindrical perforations. However, recent findings suggest that "imperfections" in the liner manufacturing process may lead to perforations that are not sharp-edged, which can strongly affect the impedance. A key experimental observation pointing to this issue is reported in Ref. [7], where 3D-printed liner samples with rounded perforation edges exhibited significantly lower resistance than that predicted by semi-empirical models. A numerical and experimental study supporting the conclusion that this behavior was caused by edge rounding is presented in Ref. [8], where a Normal Incidence Tube (NIT) configuration was used. To the best of the authors' knowledge, although studies investigating manufacturing-process effects are available in the literature [6], there is still no dedicated parametric experimental study on the effects of perforation-edge geometry on acoustic liner impedance in the presence of grazing flow.

This work addresses the lack of experimental data comparing acoustic liner impedance on the presence of grazing flow for different perforation shapes. Four liner samples were manufactured with the same nominal inner diameter (i.e., same open-area percentage), but with different hole's edge geometries, namely (i) sharp; (ii) outside chamfered; (iii) inside chamfered; and (iv) outside and inside chamfered. The acoustic liner impedance is assessed by means of two different experimental techniques at the Liner Impedance Test Rig of the Federal University of Santa Catarina (LITR/UFSC). The remainder of this document is structured as follows. Section II describes the liner samples and their geometrical characterization. Section III describes the experimental setup and test matrix. The results are presented and discussed in Section IV. Finally, the main conclusions are summarized in Section V.

II. Liner Samples

Given recent issues faced by the authors in ensuring quality and dimensional control when manufacturing 3D-printed liner samples, especially in the facesheet orifices, the liner samples in this work were machined from solid aluminum blocks using conventional manufacturing processes. Four different perforation configurations were considered: (I) a sharp-edged hole; (II) a hole with an outer chamfer; (III) a hole with an inner chamfer; and (IV) a hole chamfered on both sides. The corresponding configurations and geometric parameters used to describe the samples are shown in Fig. 1, and the nominal values for all configurations are presented in Table 1. The facesheet thickness, $t = 0.635$ mm, is constant across all configurations. Additionally, since the inner hole diameter, $d_0 = 1.0$ mm, and the number of holes per cavity are kept constant, the nominal Percentage of Open Area (POA) based on the inner diameter is also the same for all configurations.

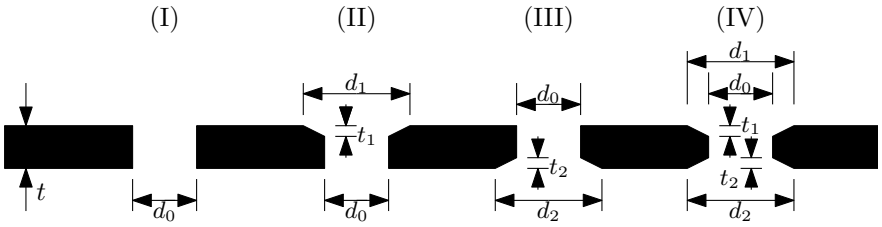

Fig. 1 Liner perforation geometries and parameters.

Table 1 Liner perforation parameters; all dimensions are in millimeters.

#	Geometry	Code	t	t_1	t_2	d_0	d_1	d_2
I	Sharp edged	SH	0.635	-	-	1.0	-	-
II	Outside Chamfered	OC	0.635	0.1	-	1.0	1.2	-
III	Internal Chamfered	IC	0.635	-	0.1	1.0	-	1.2
IV	Both sides Chamfered	DC	0.635	0.1	0.1	1.0	1.2	1.2

The samples have overall dimensions of 210 mm in length and 150 mm in height. They are composed of chambers arranged in an 8×16 cell configuration, with each cell containing 8 holes. The individual cell chambers have dimensions

of $9.9 \times 9.9\,\text{mm}^2$, with fillets of 2 mm radius at the corners to facilitate manufacturing. Hence, each cell has a POA of approximately 6.4 %. The cavity depth is $h = 38.1$ mm for all configurations.

Manufacturing limitations were imposed by the cutting tool required to produce the chamfers, which meant that the samples with chamfers facing the cavity interior could not be manufactured as a single piece. Therefore, while SH and OC were machined from a single block with depth $t + h = 38.735$ mm, IC and DC were manufactured in two pieces, such that most of the core was separated into an isolated part. More precisely, these samples were split at 8.5 mm from the facesheet, resulting in one piece with a depth of 8.5 mm (the facesheet and a small portion of the core) and another piece with a depth of 30.235 mm (the remaining portion of the cavity core). The two manufacturing approaches are illustrated in Fig. 2. Finally, to close the back of the open cavities, a thick acrylic plate was used as the back plate for the samples and was clamped only during testing.

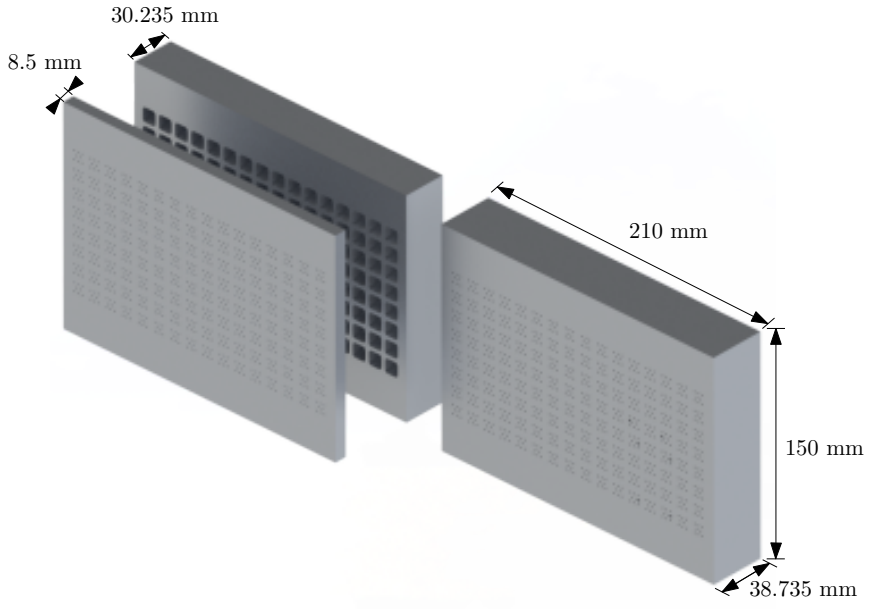

Fig. 2 Illustration of the liner samples. On the left, the sliced method for configurations (III) and (IV); on the right, the single piece method for configurations (I) and (II).

A. Geometric Optical Characterization

An optical analysis was carried out using a stereoscope to assess the actual geometry resulting from the manufacturing process. A Zeiss Stemi SV8 stereoscope equipped with a Leica camera was used, allowing the acquisition of high-resolution images. Pixel-counting methods were then applied using the software supplied by the stereoscope manufacturer.

The procedure used to obtain the perforation parameters consisted of randomly selecting 15 holes from each sample and measuring the following dimensions: (i) the external diameter, defined either as the largest chamfer diameter or as the diameter at the facesheet wall (d_1 or d_2), and (ii) the internal diameter, defined as the diameter at the midpoint of the hole, which should correspond to the smallest diameter (d_0). For the sharp-edged geometry, the internal and external diameters were assumed to be identical. For the samples manufactured in two pieces (configurations (III) and (IV)), it was also possible to obtain measurements of the internal diameter d_0 from the inner side of the liner. Afterwards, the average and standard deviation of each parameter were evaluated. The statistics obtained for all configurations and measured parameters are presented in Table 2.

It was observed that, for all chamfered configurations, the average internal diameter d_0 was smaller than the nominal value. This can be explained by the formation of small burrs during chamfer machining, which may have locally reduced the inner diameter of the orifice. Based on the semi-empirical model from Ref. [4], for the frequency and velocity ranges covered in this work (to be detailed in Section III.D), these small variations in the inner diameter may lead to variations in the normalized liner resistance smaller than 0.07 in the absence of flow, and smaller than 0.13 for the case with the maximum flow speed considered in this work, at 145 dB. Nonetheless, the external chamfer diameters were always

Table 2 Statistical data from the geometric optical characterization of the samples. All dimensions are in millimeters.

Parameter	Nominal value	Average	Standard deviation
(I) Sharp edged - SH			
d_0	1.0	1.000	0.006
(II) Outside Chamfered - OC			
d_0	1.0	0.966	0.006
d_1	1.2	1.294	0.017
(III) Inside Chamfered - IC			
$d_0\|_{\text{out}}$	1.0	1.010	0.009
$d_0\|_{\text{in}}$	1.0	0.982	0.013
d_2	1.2	1.242	0.011
(IV) Both sides Chamfered - DC			
$d_0\|_{\text{out}}$	1.0	0.990	0.009
d_1	1.2	1.273	0.018
$d_0\|_{\text{in}}$	1.0	0.984	0.011
d_2	1.2	1.258	0.013

larger than the nominal values, while remaining within manufacturing tolerances. Finally, the dimensional variation observed in the measurements was considered satisfactorily small.

III. Experimental Setup

This section presents a brief description of the experimental facilities and methods used in this work. For further details, the reader is referred to a previous publication by the authors, Ref. [9], in which both the facilities and the methods are discussed in detail.

A. Test Facilities

In this work, the LITR/UFSC was used to measure the acoustic impedance of the liner samples. A schematic representation of the facility is shown in Fig. 3. The LITR/UFSC test rig consists of a modular waveguide with a rectangular cross-section. The internal duct has a width of $W = 40\,\text{mm}$ and a height of $H = 100\,\text{mm}$. The central section is the liner sample holder, which accommodates liner samples with lengths of up to $L_{\text{liner, max.}} = 420\,\text{mm}$.

Flow is provided by a compressed-air system, which can sustain a bulk Mach number corresponding to approximately $M_{\text{max.}} \approx 0.6$. The flow velocity and temperature are measured in real time by means of a Pitot tube and a thermoresistance located immediately upstream of the test section. Loudspeakers, installed both upstream and downstream of the liner sample holder, allow for the generation of acoustic waves propagating with and against the flow, respectively. The current setup allows pure-tone acoustic waves propagating toward the liner at SPLs of up to approximately 150 dB over the frequency range from 0.5 kHz to 6.0 kHz. Flush-mounted microphones are installed on the wall opposite the liner, both upstream and downstream of the liner sample. In addition, an array of equally spaced flush-mounted microphones is installed on the wall facing the lined section, allowing the use of Prony-based eduction methods.

B. Inverse Impedance Eduction

For the purposes of this work, the acoustic propagation problem is simplified to a two-dimensional duct, as depicted in Fig. 4. Assuming a positive uniform parallel flow in the axial direction (z), with time-harmonic and axially harmonic acoustic pressure perturbations, i.e., $\tilde{p} \propto \exp(\mathrm{i}\omega t - \mathrm{i}k_z z)$, the acoustic field is governed by the Convected Helmholtz Equation,

$$\left(\nabla_\perp^2 + (k - Mk_z)^2 - k_z^2\right)\tilde{p} = 0, \tag{1}$$

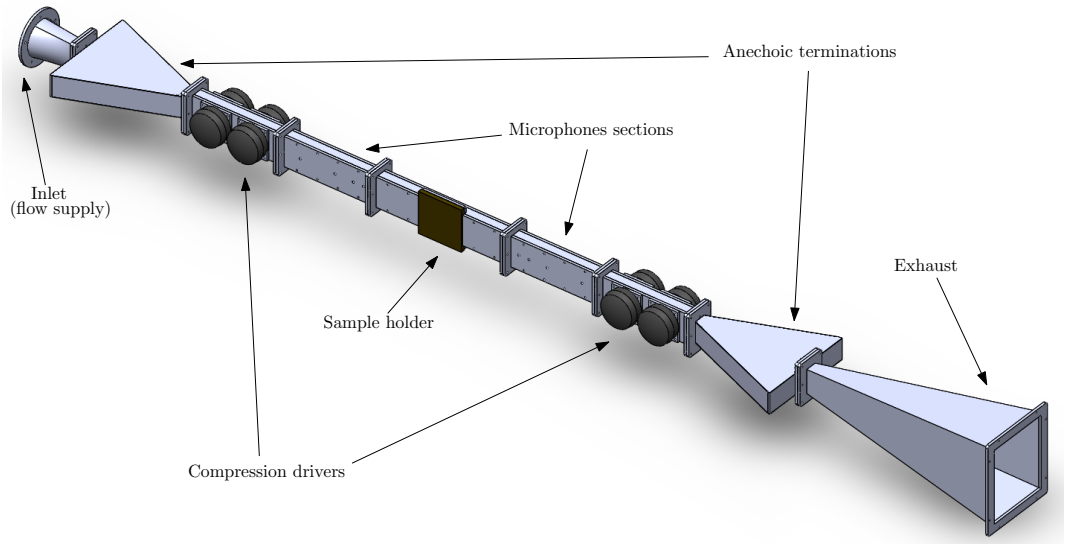

Fig. 3 Schematic representation of the LITR/UFSC.

where $M \equiv U/c_0$ is the bulk Mach number, c_0 is the speed of sound, $k = \omega/c_0$ is the free-field wavenumber, and k_z is the axial wavenumber. In this work, under the two-dimensional duct assumption, $\nabla_\perp^2 \equiv \frac{\mathrm{d}^2}{\mathrm{d}x^2}$.

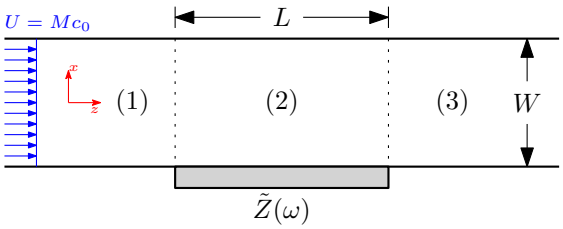

Fig. 4 Two-dimensional waveguide and coordinate system adopted in this work.

At each section j, the acoustic field $\tilde{p}(x,z)$ can be approximated by a sum of $\mathcal{N}$ acoustic modes,

$$\tilde{p}^{(j)}(x,z) = \sum_{n=1}^{\mathcal{N}} \left(A_n^{(j)+} \psi_n^{(j)+}(x) \exp\left(-\mathrm{i} k_{z,n}^{(j)+} z\right) + A_n^{(j)-} \psi_n^{(j)-}(x) \exp\left(-\mathrm{i} k_{z,n}^{(j)-} z\right) \right), \tag{2}$$

where A_n are the modal amplitudes, $\psi_n(x)$ are the mode shapes, and the superscripts + and − denote downstream- and upstream-propagating modes, respectively.

At the majority of the duct walls, the rigid wall boundary condition implies $\frac{\mathrm{d}\tilde{p}}{\mathrm{d}x} = 0$. On the other hand, at the lined wall, the Ingard–Myers Boundary Condition (IMDC) [10, 11] is assumed,

$$\frac{\mathrm{d}\tilde{p}}{\mathrm{d}x} = \frac{\mathrm{i}}{kZ}(k - Mk_z)^2 \tilde{p}. \tag{3}$$

For the frequency range and microphone locations considered here, the modal amplitudes in the rigid-walled sections can be determined by means of a plane-wave decomposition. This can be carried out using an overdetermined decomposition procedure, for example, in the upstream section,

$$\begin{bmatrix} \exp\left(-\mathrm{i}k_{z,1}^{+} z_1\right) & \exp\left(-\mathrm{i}k_{z,1}^{-} z_1\right) \\ \exp\left(-\mathrm{i}k_{z,1}^{+} z_2\right) & \exp\left(-\mathrm{i}k_{z,1}^{-} z_2\right) \\ \exp\left(-\mathrm{i}k_{z,1}^{+} z_3\right) & \exp\left(-\mathrm{i}k_{z,1}^{-} z_3\right) \\ \exp\left(-\mathrm{i}k_{z,1}^{+} z_4\right) & \exp\left(-\mathrm{i}k_{z,1}^{-} z_4\right) \end{bmatrix} \begin{bmatrix} A_1^{+} \\ A_1^{-} \end{bmatrix} = \begin{bmatrix} \tilde{p}_1 \\ \tilde{p}_2 \\ \tilde{p}_3 \\ \tilde{p}_4 \end{bmatrix}, \tag{4}$$

and similarly for the downstream section. The plane-wave axial wavenumber, $k_{z,1}^{\pm} = \pm kK_0/(1 \pm K_0 M)$, also accounts for viscothermal losses at the duct walls through the first-order Kirchhoff solution K_0 [12]. Afterwards, the modal amplitudes in the lined section can be determined by enforcing continuity of mass and momentum at each interface, following Ref. [13]. This procedure is known in the literature as the Mode Matching Method (MMM).

The lined-wall impedance is obtained through an iterative procedure. An initial impedance guess is required to compute the theoretical acoustic field p_q^{num} at each microphone location z_q, which is then compared with the measured acoustic field p_q^{exp} by means of the following cost function

$$\mathcal{F}(Z) = \sum_{q=1}^{Q} \left| \frac{\tilde{p}_q^{\text{exp}} - \tilde{p}_q^{\text{num}}(Z)}{\tilde{p}_q^{\text{exp}}} \right|, \tag{5}$$

where $Q = 8$ is the total number of microphones. The Levenberg–Marquadt algorithm [14, 15] is used to minimize this cost function, yielding the liner impedance. In order to accelerate convergence, the semi-empirical impedance model from Ref. [4] is employed as the initial guess for the liner impedance.

C. In-Situ Technique

The in-situ measurement technique estimates the acoustic liner impedance from measurements of the acoustic pressure at the facesheet and at the rigid backing plate of a liner cell. The in-situ technique implicitly assumes that the liner is locally reactive, and no assumptions are made regarding the flow outside the liner. Therefore, it does not rely on the definition of a boundary condition such as the Ingard–Myers boundary condition [10, 11], since it does not attempt to model the acoustic field as in impedance-eduction techniques.

The main assumptions of the in-situ technique are that: (i) the backplate is perfectly reflective; (ii) only standing plane waves exist in the cell; and (iii) the facesheet is acoustically thin, so that the acoustic particle velocity is the same on both sides of the facesheet [16]. Under these conditions, it can be shown that the in-situ impedance is given by

$$\tilde{Z} = \frac{-\mathrm{i}\tilde{H}_{\text{fb}}}{\sin(kh)}, \tag{6}$$

where $\tilde{H}_{\text{fb}}$ is the ratio between the complex acoustic pressures at the facesheet and the backplate, and h is the cavity height. In practice, $\tilde{H}_{\text{fb}}$ is determined from the transfer function between the complex acoustic pressures at the facesheet and the backplate. In this work, the capillary-probe approach described in Ref. [9] is used. The effect of the instrumentation on the measured impedance is corrected using

$$\tilde{Z}_{\text{liner}} = \frac{\tilde{Z}_{\text{meas}} + \mathrm{i}\cot(kh)}{1 - \varepsilon_w - \varepsilon_m} + \mathrm{i}\frac{\varepsilon_m}{\tan(kh)} - \mathrm{i}\cot(kh). \tag{7}$$

where $\tilde{Z}_{\text{meas}}$ is the measured impedance obtained from Eq. (6); ε_w is the ratio between half of the cross-sectional area of the surrounding cell walls and the area of the liner cell; and ε_m is the ratio between the blocked volume due to instrumentation and the cell volume.

D. Test Matrix

In this work, the flow conditions are defined in terms of the centerline Mach number, M_{c}, which corresponds to the maximum flow velocity in the duct cross-section. Three flow conditions are considered: (i) the no-flow case, $M_{\text{c}} = 0.00$; (ii) $M_{\text{c}} = 0.32$; and (iii) $M_{\text{c}} = 0.50$, which correspond to bulk Mach numbers of $M = 0.000$, 0.272, and 0.436, respectively.

The acoustic excitation consisted of a pure-tone signal ranging from 500 Hz to 3000 Hz in 100 Hz increments. The acoustic source was positioned either upstream or downstream of the liner, with only one propagation direction considered at a time. The SPL was defined based on the amplitude of the plane wave propagating toward the liner, and the source power was adjusted such that the SPL was either 130 dB or 145 dB for the cases with $M_{\text{c}} = 0.00$ and $M_{\text{c}} = 0.32$, and 145 dB for the case with $M_{\text{c}} = 0.50$, in order to ensure adequate signal-to-noise ratio under the highest-flow condition.

The impedance-eduction method was applied to all operating conditions and perforation configurations. However, the instrumentation of the sliced samples (IC and DC) was found to be nontrivial, making it difficult to ensure proper probe alignment and sealing. Therefore, the in-situ technique was applied only to the SH and OC configurations.

Moreover, recent findings from high-fidelity numerical simulations of acoustic liners suggest that the impedance measured using the in-situ technique is strongly dependent on facesheet-probe positioning. Therefore, in this work, two adjacent cells were instrumented. These cells are located in the third column and in the middle rows of the sample. In one of them, the additional hole for the facesheet probe was positioned upstream of the cavity holes, whereas in the other it was positioned downstream of them, as schematically depicted in Fig. 5. The impedance obtained for both cavities was then averaged to obtain the final result. Furthermore, the samples were rotated between measurements with upstream and downstream source excitation, so that the instrumented cell was always located at the sample edge nearest to the acoustic source.

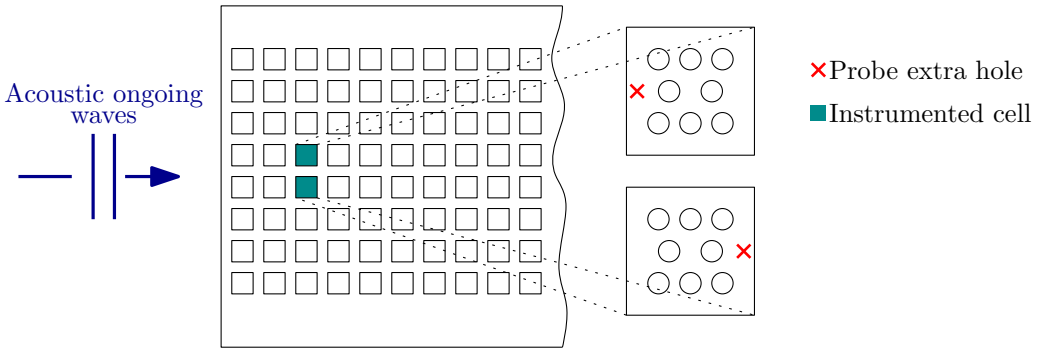

Fig. 5 Representation of the location of the instrumented cells for the in-situ technique and the facesheet-probe hole location.

IV. Results and Discussion

The reader may have noticed that the test matrix of this study is substantially large. However, the main conclusions can be drawn from a much smaller subset of cases. Therefore, for the sake of brevity, only a representative set of results is presented in this document, while the complete dataset will be made publicly available in an open-source format. Unless otherwise stated, the results shown in the remainder of this document correspond to the upstream acoustic source configuration, which provides the clearest comparison between configurations. The results obtained with the opposite source arrangement were found to be qualitatively consistent with the same trends. In addition, for the inverse impedance-eduction method, only the cases with $M_c = 0.00$ and $M_c = 0.32$ are considered, since the accuracy of the assumed IMBC decreases significantly for $M_c = 0.50$ [17, 18]

First, the results obtained with the inverse impedance-eduction method are analyzed. Figure 6 shows the results obtained for the no-flow case at both 130 dB and 145 dB, for all configurations. The results suggest that, as expected, in the absence of mean flow, the reactance is not significantly affected by the different perforation configurations, since it is mainly governed by the cavity geometry. At 130 dB, all configurations still show broadly similar resistance levels, although a slightly lower resistance is already observed for the both-sides chamfered (DC) configuration. This indicates that the sensitivity of acoustic liner resistance to perforation-edge shape is already present under no-flow conditions at 130 dB, in agreement with previous observations reported in Ref. [8], but remains substantially weaker than that observed at 145 dB.

On the other hand, the results obtained at 145 dB suggest a strong dependence on perforation-edge shape when nonlinear effects become relevant, in agreement with previous reports in the literature [8]. This pattern is especially clear in the mid-frequency range (1500 Hz $< f <$ 2500 Hz), where the resistance levels can be ordered as SH>OC>IC>DC. One may notice that the resistance decreases as the number of sharp edges explicitly decreases. This suggests that the acoustic viscous dissipation during the inflow and outflow stages at the liner orifices is strongly affected by perforation-edge geometry. One possible explanation is the increase in the discharge coefficient associated with the presence of chamfers.

One may notice that, at the lower-frequency end, the IC configuration displays a higher resistance than the OC configuration, whereas the opposite is observed at the higher-frequency end. Further investigation is required to explain this frequency-dependent behavior, and a dedicated numerical analysis may help clarify the underlying mechanisms. However, it may be related to the wave-incidence angle, which changes from grazing on the outer side to normal on the inner side, combined with the liner resonance, which is around 1400 Hz for the samples considered in this study.

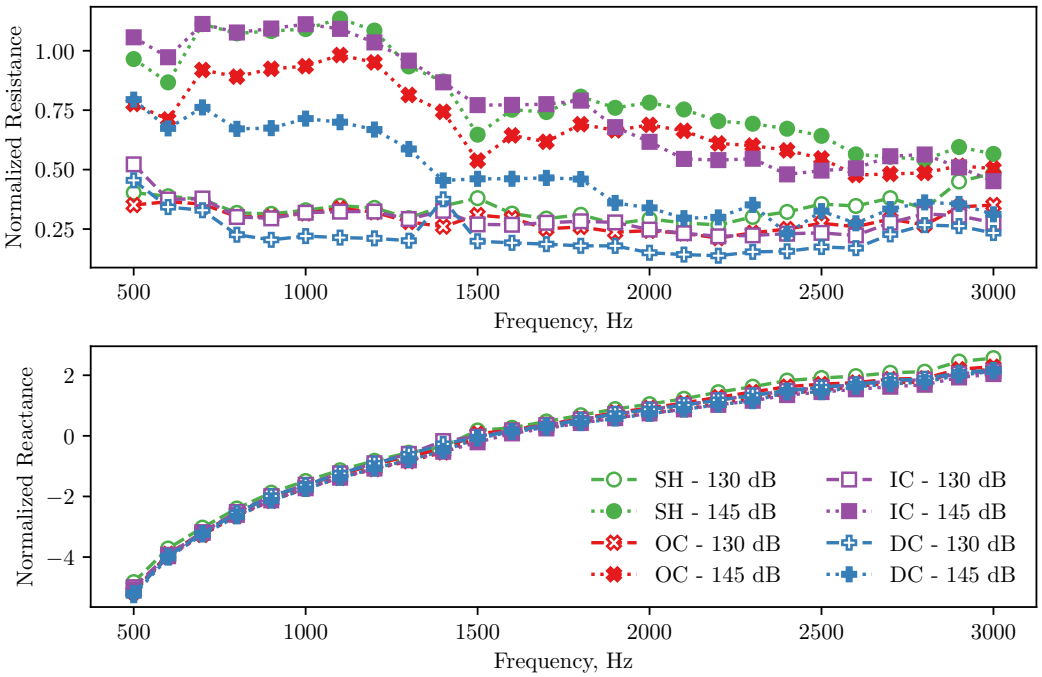

Fig. 6 Impedances educed with $M_c = 0.00$.

Figure 7 displays the results obtained for a flow condition with $M_c = 0.32$, for all perforation configurations and both SPLs considered. The results suggest that, as in the no-flow case, the perforation-edge geometry has no significant effect on the reactance, although small differences are observed at the lower-frequency end for the configurations with internal chamfering (IC and DC).

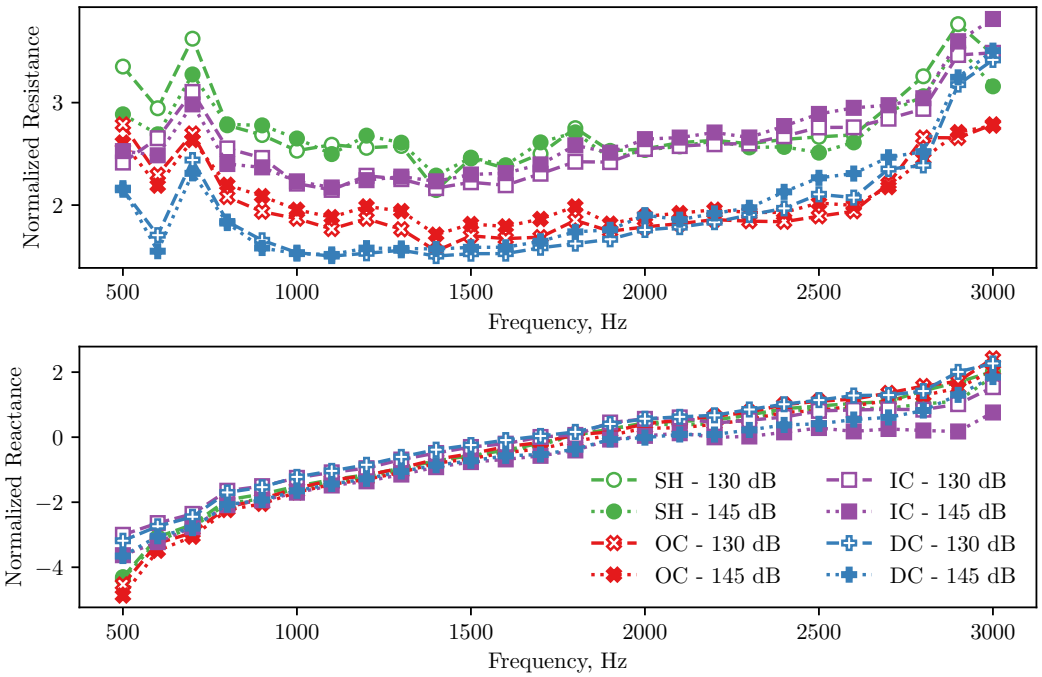

Fig. 7 Impedances educed with $M_c = 0.32$.

In the presence of grazing flow, the educed impedances are not significantly influenced by SPL-induced nonlinear effects, in agreement with previous findings reported in Ref. [19], since the nonlinear effects induced by the grazing flow become dominant. A clear reduction in resistance associated with the presence of an outer chamfer at the facesheet holes is observed, as indicated by the significantly lower resistance values obtained for the OC and DC cases. Furthermore, the inner chamfer also appears to contribute to a reduction in liner resistance, since the DC and IC cases exhibit lower resistance than their corresponding counterparts with only an outer chamfer or no chamfer, namely OC and SH, respectively.

Finally, the results obtained with the in-situ technique are presented in Fig. 8, allowing the analysis to be extended to higher mean-flow velocities. These results confirm the main trends observed in the impedance-eduction results: (i) the nonlinear effects induced by grazing flow dominate over those associated with SPL; (ii) the reactance is not significantly affected by the presence of chamfers at the perforation edges; and (iii) the presence of an outer chamfer significantly reduces the nonlinear increase in liner resistance associated with grazing flow.

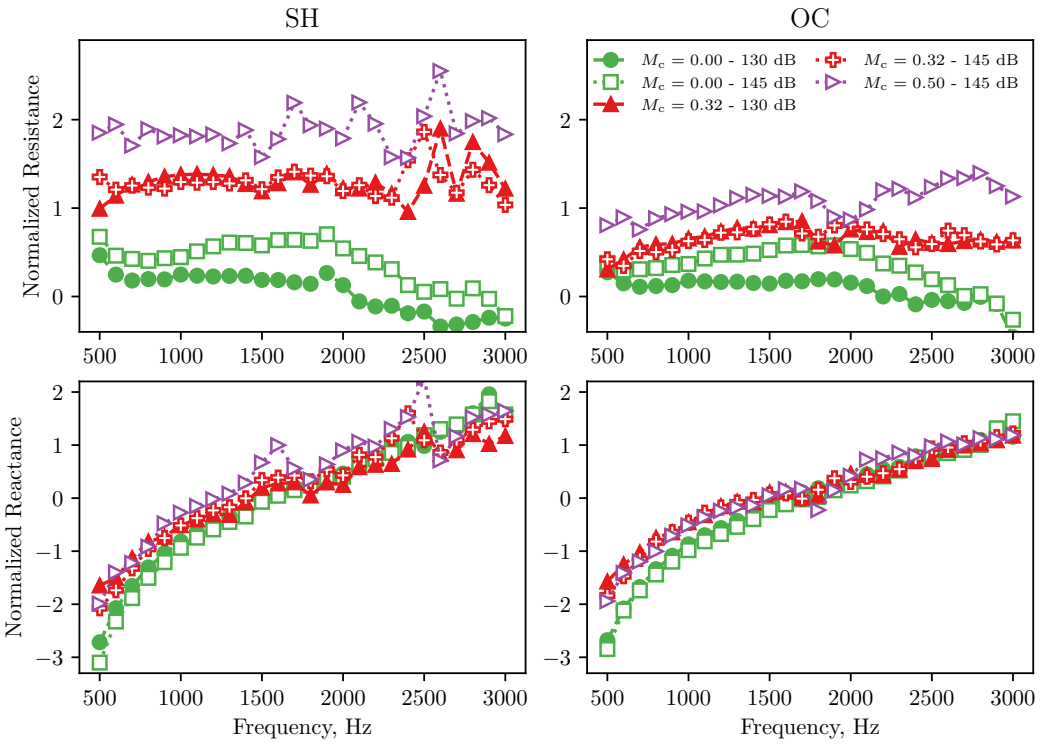

Fig. 8 Impedances obtained with the in-situ technique. On the left, results for SH; on the right, results for OC.

V. Concluding Remarks

The effects of perforation-edge geometry on the impedance of SDOF acoustic liners were investigated. Four different configurations were considered, namely sharp-edged (SH), outside-chamfered (OC), internally chamfered (IC), and both-sides chamfered (DC). Two different experimental techniques were employed to assess the sensitivity of liner impedance to these configurations under varying grazing-flow velocities and SPLs.

The results suggest that the reactance is not significantly affected by perforation-edge geometry, as expected, since this quantity is governed primarily by the liner cavities. In the absence of flow, it was observed that the presence of chamfers in the perforations can reduce the nonlinear resistance induced at high SPLs. There are still open questions regarding the fact that the presence of an internal chamfer leads to lower resistance than an external chamfer in some cases, and further investigation is left for future work.

In the presence of grazing flow, the nonlinear resistance induced by the flow dominates over the effects associated with SPL, and it was found that the presence of outer chamfers can lead to significantly lower resistance. This work aimed to help fill a gap in the literature by providing experimental data on the effects of chamfered edges on SDOF liner

acoustic impedance, although some questions remain open. For instance, it is still uncertain whether the reduction in resistance is caused by the chamfer itself or by the larger external diameter. These questions may be addressed in future work by including conical holes, which would allow a gradual variation from the external to the internal diameter. Rounded edges should also be considered, as they would lead to smoother transitions between the internal and external diameters, although for the NIT it was found that edge rounding may lead to effects similar to those caused by chamfers [8]. Further studies may also include a parametric analysis of the POA and internal hole diameter, d_0.

Acknowledgments

This work was partially supported by the AeroAcoustics Research Consortium (AARC). The AARC is a government-industry partnership supporting pre-competitive research for aircraft noise reduction. J. A. Cordioli acknowledges funding from the Brazilian funding agency CNPq (National Council for Scientific and Technological Development) through the process 315000/2021-0. The work of F. Avallone is co-funded by the European Union (ERC, LINING, 101075903). Views and opinions expressed are however those of the author(s) only and do not necessarily reflect those of the European Union or the European Research Council. Neither the European Union nor the granting authority can be held responsible for them.

References

[1] Smith, M. J. T., *Aircraft noise*, Cambridge University Press, UK, 1989.

[2] Paduano, A., Scarano, F., Cordioli, J., Casalino, D., and Avallone, F., "On the impact of the turbulent grazing flow development on the acoustic response of an acoustic liner," , Jul. 2025. https://doi.org/10.48550/arXiv.2507.22714, arXiv:2507.22714 [physics].

[3] Guess, A. W., "Calculation of perforated plate liner parameters from specified acoustic resistance and reactance," *Journal of Sound and Vibration*, Vol. 40, No. 1, 1975, pp. 119–137. https://doi.org/10.1016/S0022-460X(75)80234-3.

[4] Yu, J., Ruiz, M., and Kwan, H. W., "Validation of Goodrich perforate liner impedance model using NASA langley test data," *14th AIAA/CEAS Aeroacoustics Conference (29th AIAA Aeroacoustics Conference)*, Vancouver, British Columbia, Canada, 2008. https://doi.org/10.2514/6.2008-2930.

[5] Cerizza, D., and Casalino, D., "An Indirect Impedance Eduction Process for Liners with Arbitrarily Complex Geometry," *AIAA AVIATION Forum*, American Institute of Aeronautics and Astronautics, San Diego, CA, USA, 2023. https://doi.org/10.2514/6.2023-4186.

[6] Murray, P., Ferrante, P., and Scofano, A., "Manufacturing process and boundary layer influences on perforate liner impedance," *11th AIAA/CEAS aeroacoustics conference*, American Institute of Aeronautics and Astronautics, Monterey, California, 2005. https://doi.org/10.2514/6.2005-2849.

[7] Quintino, N. T., Bonomo, L. A., Cordioli, J. A., Jones, M. G., Howerton, B. M., Nark, D. M., and Avallone, F., "Comparison of Impedance Eduction Test Rigs with Different Boundary-Layer Profiles," *AIAA Journal*, Vol. 63, No. 11, 2025, pp. 4872–4883. https://doi.org/10.2514/1.J065173.

[8] Avallone, F., Khedr, A., Paduano, A., Scarano, F., Meirelles, L., and Cordioli, J., "On the Relevance of Facesheet Orifice Geometry to Acoustic Liner Impedance," *npj Acoustics*, Vol. 2, No. 1, 2026, p. 6. https://doi.org/10.1038/s44384-026-00044-x.

[9] Bonomo, L., Quintino, N., Spillere, A., Murray, P., and Cordioli, J., "A comparison of in situ and impedance eduction experimental techniques for acoustic liners with grazing flow and high sound pressure level," *International Journal of Aeroacoustics*, Vol. 23, 2024. https://doi.org/10.1177/1475472X231225629.

[10] Ingard, U., "Influence of Fluid Motion Past a Plane Boundary on Sound Reflection, Absorption, and Transmission," *The Journal of the Acoustical Society of America*, Vol. 31, 1959, pp. 1035–1036. https://doi.org/10.1121/1.1907805.

[11] Myers, M. K., "On the Acoustic Boundary Condition in the Presence of Flow," *Journal of Sound and Vibration*, Vol. 71, 1980, pp. 429–434. https://doi.org/10.1016/0022-460X(80)90424-1.

[12] Dokumaci, E., "Sound transmission in narrow pipes with superimposed uniform mean flow and acoustic modelling of automobile catalytic converters," *Journal of Sound and Vibration*, Vol. 182, No. 5, 1995, pp. 799 – 808. https://doi.org/10.1006/jsvi.1995.0233.

[13] Gabard, G., and Astley, R., "A computational mode-matching approach for sound propagation in three-dimensional ducts with flow," *Journal of Sound and Vibration*, Vol. 315, No. 4, 2008, pp. 1103 – 1124. https://doi.org/10.1016/j.jsv.2008.02.015.

[14] Levenberg, K., "A method for the solution of certain non-linear problems in least squares," *Quarterly of Applied Mathematics*, Vol. 2, No. 2, 1944, pp. 164–168. https://doi.org/10.1090/qam/10666.

[15] Marquardt, D. W., "An Algorithm for Least-Squares Estimation of Nonlinear Parameters," *Journal of the Society for Industrial and Applied Mathematics*, Vol. 11, No. 2, 1963, pp. 431–441. https://doi.org/10.1137/0111030.

[16] Dean, P., "An in situ method of wall acoustic impedance measurement in flow ducts," *Journal of Sound and Vibration*, Vol. 34, No. 1, 1974, pp. 97 – IN6. https://doi.org/10.1016/S0022-460X(74)80357-3.

[17] Yang, J., Humbert, T., Golliard, J., and Gabard, G., "Shear flow effects in a 2D duct: Influence on wave propagation and direct impedance eduction," *Journal of Sound and Vibration*, Vol. 576, 2024, p. 118296. https://doi.org/10.1016/j.jsv.2024.118296.

[18] Bonomo, L. A., Brambley, E. J., and Cordioli, J. A., "Effects of the sheared flow velocity profile on impedance eduction in a 2D duct," *Acta Acustica*, Vol. 10, 2026, p. 6. https://doi.org/10.1051/aacus/2026005.

[19] Bonomo, L. A., Quintino, N. T., Spillere, A. M. N., Murray, P. B., and Cordioli, J. A., "A comparison of in situ and impedance eduction experimental techniques for acoustic liners with grazing flow and high sound pressure level," *International Journal of Aeroacoustics*, 2024, p. 1475472X231225629. https://doi.org/10.1177/1475472X231225629.